

# Kinematics of the Local Universe

## V. The value of $H_0$ from the Tully-Fisher $B$ and $\log D_{25}$ relations for field galaxies

G. Theureau<sup>1</sup>, M. Hanski<sup>2</sup>, T. Ekholm<sup>2</sup>, L. Bottinelli<sup>1,3</sup>, L. Gouguenheim<sup>1,3</sup>, G. Paturel<sup>4</sup>, and P. Teerikorpi<sup>2</sup>

<sup>1</sup> Observatoire de Paris-Meudon, CNRS URA1757, F-92195 Meudon Principal Cedex, France

<sup>2</sup> Tuorla Observatory, FIN-21500 Piikkiö, Finland

<sup>3</sup> Université Paris-Sud, F-91405 Orsay, France

<sup>4</sup> Observatoire de Lyon, F-69230 Saint-Genis Laval, France

Received 29 July 1996 / Accepted 9 December 1996

**Abstract.** We have studied the value of the Hubble constant using the KLUN (Kinematics of the Local Universe) sample of 5171 spiral galaxies having isophotal diameters  $D_{25}$  (and partially  $B$ -magnitudes), H I line widths, and radial velocities. The sample is diameter-limited, complete down to  $D_{25} = 1.6$  arcmin. As in the first similar study, where a much smaller magnitude-limited sample was used (Bottinelli et al. 1986), we pay special attention to the problem of Malmquist bias when photometric distances are derived by the Tully-Fisher diameter or magnitude relations. The bias is revealed and overcome by a more advanced version of the method of normalized distances, now taking into account, in addition to diameter and magnitude limits, also Hubble type effect, inclination effect, and variable galactic extinction.

Calibration of the Tully-Fisher relations is primarily performed using a sample of 15 galaxies with available Cepheid distances, mostly from the HST programmes. This sample does not show significant trends with distance and is concluded to be closely distance-limited.

Analysis of the  $\log H_0$  vs.  $d_{\text{normalized}}$  diagrams allows us to identify the “unbiased plateaus” for both the diameter and magnitude TF distances. A useful tool here introduced is the theoretical expectation of the bias in cumulative  $\langle \log H_0 \rangle$  as a function of the fraction of the sample accepted for the plateau. An iterative approach is utilized for determining the TF relations, the plateau, and the value of  $H_0$  therefrom.

Using the Peebles linear velocity field model with Virgo and our infall velocities equal to  $980 \text{ km s}^{-1}$  and  $150 \text{ km s}^{-1}$ , respectively, we derived the following values of  $H_0$ :

$$H_0 = 53.4 \pm 5.0 \text{ km s}^{-1} \text{ Mpc}^{-1} (N_{\text{gal}} = 415)$$

from the magnitude relation, and

$$H_0 = 56.7 \pm 4.9 \text{ km s}^{-1} \text{ Mpc}^{-1} (N_{\text{gal}} = 403)$$

from the diameter relation.

The given  $1 \sigma$ -errors refer to the statistical scatter around the adopted calibration, and the dispersion of the calibrator sample itself. These  $H_0$  values are not sensitive to reasonable changes in the kinematical parameters of the velocity field model, up to the extreme ones found in literature. This insensitivity is also expected from our numerical experiments. In the radial velocity space, the unbiased plateau extends up to about  $6000 \text{ km s}^{-1}$  and the value of  $H_0$  is in good agreement with the SNIa results by Sandage et al. (1996) which extend to still larger velocities. At present, the supernovae method and the KLUN TF-sample, both calibrated with Cepheid distances, provide complementary approaches to  $H_0$  in different, though overlapping, redshift ranges.

As an additional result, the normalized distance method provides a natural way to estimate the Local Group infall velocity by minimizing the  $\log H_0$  dispersion in the unbiased plateau. Using the diameter and the magnitude TF relations respectively, we obtained, as preliminary results, the following values:

$$v_0 = 225 \pm 45 \text{ km s}^{-1}, \text{ and}$$

$$v_0 = 185 \pm 40 \text{ km s}^{-1}$$

These values are compatible with our standard value within  $2 \sigma$  and agree particularly well with Sandage’s preferred value  $v_0 = 220 \text{ km s}^{-1}$ .

**Key words:** galaxies: spiral – galaxies: distances and redshifts – cosmology: distance scale

---

### 1. Introduction

About ten years ago we published a paper on the Malmquist bias and the value of the Hubble constant, as revealed by the  $B_t^0$  Tully-Fisher (TF) relation (Bottinelli et al. 1986, or BGPT86).

In that paper the method of normalized distances was for the first time applied to a sample of galaxies in an attempt to show the very existence of and to correct for the Malmquist bias when the value of  $H_0$  is derived from field galaxies using the direct TF relation. The method accomplishes simultaneously these two tasks via the  $\log H$  vs.  $d_n$  diagram, where  $H$  is the Hubble ratio  $V_c/d_{TF}$  ( $V_c$  = corrected radial velocity,  $d_{TF}$  = TF distance from the direct TF relation) and  $d_n$  is the normalized kinematical distance (we shall return to the details in Sect. 3).

BGPT86 illustrated in a clear manner how the Malmquist bias influences the inferred value of  $H_0$ . The value of  $H_0$  was derived from the “unbiased plateau” of the  $\log H$  vs.  $d_n$  diagram, using the calibrators then available. With two choices of calibrator distances we calculated  $H_0 = 72 \pm 3 \text{ km s}^{-1} \text{ Mpc}^{-1}$  and  $H_0 = 56 \pm 3 \text{ km s}^{-1} \text{ Mpc}^{-1}$ , where the former value refers to the “short” (or de Vaucouleurs) distances and the latter one to the “long” (or Sandage) distances, in use at that time. It is the aim of the present paper to “update” in a very basic manner the results of BGPT86, after ten years of efforts by us and others to increase the data base, enhance the knowledge of the TF relation, and deepen the understanding of the Malmquist bias.

After BGPT86 it became clear that in order to put the investigation of  $H_0$  and the local kinematics on a safer basis, when using the basic  $B_t^0$  (or  $\log D_{25}$ ) photometric parameters in the TF relation, one needs a significantly larger sample than available in 1986. There are several reasons for this. *Firstly*, the method of normalized distances requires complete samples, and to extend the unbiased plateau requires fainter photometric limit. *Secondly*, increasing the population of the unbiased plateau adds weight on  $H_0$  from increasingly large distances, hence reducing the influence of the very local kinematical environment. *Thirdly*, the larger number of galaxies allows one to investigate in detail the properties of the sample, its completeness, and needed photometric corrections. *Fourthly*, similarly, the large sample makes it possible to study the TF-relation itself. *Fifthly*, though our main concern is the direct relation, any attempt to use the inverse TF relation (producing in a certain sense unbiased distance moduli) requires a good, homogeneous and well-understood photometric sample, along with the complete measurements of  $\log V_m$ .

The roots of this work go back to 1983 when a plan was started to build an extragalactic database (Paturel et al. 1990) where the basic available measurements would be collected. This database (LEDA = Lyon-Meudon extragalactic database; telnet *lmc.univ-lyon1.fr*, login: *leda*) contains presently 140000 galaxies which have been used to homogenize the data relevant for TF studies. This part of the work has been reported by Bottinelli et al. (1990), Paturel et al. (1991a), and Paturel et al. (1994a), concerning 21-cm line measurements ( $\log V_m$ ), apparent diameters, and total apparent magnitudes, respectively.

In the project “Kinematics of the local universe” (KLUN), we have constructed a large sample of TF suitable galaxies, complete down to a small apparent diameter (Paturel et al. 1990). We selected diameter instead of magnitude as the defining parameter, because in this way it was possible to create with tolerable effort a deep sample, and because diameters also obey a TF re-

lation. In fact, as a very useful byproduct of this project, it was also possible to make the magnitude limit fainter within the basic diameter-limited sample. Completing the sample required several hundreds of H I line profile measurements with the Nançay radiotelescope and hundreds of optical redshift measurements at Observatoire de Haute Provence and at ESO, La Silla, as a Key Project.

Preparations for the KLUN analysis have included a study of the inclination corrections by Bottinelli et al. (1995), where it was shown that the isophotal diameter changes very little when the viewing angle is changed (consistent with a high optical thickness of spiral galaxy disks at the 25 mag isophote), while  $B$ -magnitudes need a large correction. Another important preparative study concerned the type dependence of the TF relation. It was revealed especially using the inverse TF relations in Theureau et al. (1997), but it exists as well in the direct relations, both in diameters and magnitudes.

The Malmquist bias has received increasing attention during the last ten years, with advancement in our understanding of its different forms and situations in which it enters the results. Teerikorpi (1995) recommended the use of the terms “Malmquist bias of the 1st kind” and “Malmquist bias of the 2nd kind”, in order to make a clear difference between two approaches in the studies using distance measurements. The bias of the 2nd kind is the one that arises in the analysis of the  $\log H$  vs.  $d_n$  diagram and which we try to overcome using the method of normalized distances. It is also the bias that Sandage (1994a,b) has discussed with his approach via the Spaenhauer diagram. The bias of the 1st kind is closely akin to the classical Malmquist bias, and has appeared in discussions on the “general” Malmquist correction.

Our approach to  $H_0$  relies on a *sufficiently* good velocity field model that is used to calculate (relative) kinematical distances. In 1986 we used the Peebles linear model, centered around the Virgo cluster, for this purpose. Even though the years have brought about new information on possible large scale bulk flows (starting from the Hydra Centaurus flow as suggested by Tammann & Sandage 1985) and the possible Great Attractor infall flow (Lynden-Bell et al. 1988), we shall use the same basic kinematical model also in this study, which allows a comparison with the results of BGPT86.

Presently, the number of local calibrators with distances from primary indicators is significantly larger than in 1986. Our complete list contains now 30 local galaxies, half of them having primary Cepheid measurements, the other half with distances determined by group membership. It should be noted that 11 of the new primary (Cepheid) distances come from the HST programmes.

We outline below the structure of this paper:

In Sect. 2, the basic KLUN sample is described. The criteria for excluding parts of the sample due to problems of galactic extinction, kinematical closeness of the Virgo cluster, and inaccurate photometric parameters, are explained.

In Sect. 3, the method of normalized kinematical distances is explained, with some improvements in comparison with

BGPT86. The comparable method of the Spaenhauer diagram (Sandage, 1994a) is discussed.

In Sect. 4, possible calibrators are discussed. We have decided to give two choices of calibrator sample: a smaller primary sample of galaxies with Cepheid distances, and a sample enlarged with group members.

In Sect. 5, we use both the diameter-limited sample, and the magnitude-limited subsample, in the iterative normalized distance method. We derive the slope of the TF relations, zero-point differences for the Hubble types, and the unbiased plateau in the  $\log H$  vs.  $d_n$  diagram. Systematic trends inside the putative plateaus, defined by different  $d_n$ -limits, are studied. All this can be done without a knowledge of  $H_0$  (or of calibrators).

In Sect. 6, we combine the data on calibrators with the results on the unbiased plateaus from Sect. 5, in order to derive the value of the Hubble constant. The calculations are made with different calibrator samples, and with different plateaus from Sect. 5.

Sect. 7 contains a discussion of the results on  $H_0$ . We investigate the effect of the adopted velocity model, absorption correction, and absolute calibration. We conclude by comparing our results with recent SNIa studies.

## 2. The KLUN sample

The galaxy sample that we use is basically the same that we have collected and investigated in a few previous papers of the “Extragalactic Data Base” (Paturel et al. 1989, Bottinelli et al. 1990, Paturel et al. 1991a, 1991b, 1994a, Bottinelli et al. 1995) and “Kinematics of the Local Universe” series (Paturel et al. 1994b, Bottinelli et al. 1992, 1993, Di Nella et al. 1996, Theureau et al. 1997). In totality it consists of 5171 spiral galaxies covering the type range Sa - Sdm (or  $T = 1 - 8$ ). Each galaxy has a photometric diameter ( $\log D_{25}$ ), a 21-cm line width and a radial velocity measurement. 4577 of these objects have also  $B$ -magnitudes.

Any derivation of  $H_0$  using such a data base, depends crucially on our knowledge of the statistical properties of the sample, including its incompleteness and the quality of the measured parameters. The KLUN sample has its origin in a merger of several galaxy catalogues, with the original photometric measurements made in different ways and accuracies. This makes it necessary to practice special care when the formal methods are applied to the sample.

### 2.1. Diameters

Diameters  $D_{25}$  are expressed in units of  $0''.1$ , with an accuracy of  $0''.01$ , following the convention of the RC2 (de Vaucouleurs et al. 1976). They are extracted from LEDA and have been reduced to a standard common system according to Paturel et al. (1991a): isophotal diameters at the limiting surface brightness of  $25 B$ -mag (arc sec) $^{-2}$ . For most of the sample, the standard error of  $\log D_{25}$  does not exceed  $\sigma = 0.05$ . Diameters were corrected for galactic extinction (Fouqué and Paturel, 1985) and inclination effect (Bottinelli et al. 1995).

The sample can be considered complete in observed diameter down to  $\log D_{\text{lim}} = 1.2$  (for details, see Paturel et al. 1994b).

The  $D_{25}$  diameter is measured in most cases in the disc only (Theureau et al. 1997). Hence, the diameter limit is roughly the same for all morphological types.

### 2.2. Magnitudes

The reduction of apparent  $B$ -magnitudes to the RC3 (de Vaucouleurs et al. 1991) system has been studied recently by Paturel et al. (1996). The mean  $B_t$  is an average with the weights derived for each source of magnitude. The final uncertainty is derived from the total weight. In most of the sample, the standard error is less than 0.5 mag.

Apparent  $B_t$  magnitudes are corrected for galactic extinction ( $a_g$ ), inclination and redshift effects, according to Bottinelli et al. (1995). We adopted for  $a_g$  the RC2 system (see Sect. 7.2.).

The whole sample is complete below  $m_{\text{lim}} = 13.25$  mag. It is important to note, that because the sample is diameter-limited and the magnitudes are correlated with the size of the bulge component for a fixed intrinsic diameter, the magnitude limit  $m_{\text{lim}}$  will be different for different galaxy types. In fact, for a given completeness limit in diameter  $D_{\text{lim}}$ , one obtains, from the exponential law, the following expression:

$$m_{\text{lim}} = -2.5 \log \left[ \frac{2\pi\sigma_0}{1 - k(T)} \left( \frac{D_{25,\text{lim}}}{6.4} \right)^2 \right] + M_{\odot} - 5, \quad (1)$$

where  $k(T)$  is the bulge to disc luminosity ratio for a given type, as given by Simien & de Vaucouleurs (1986), and  $\sigma_0 = 10^{-0.4\mu_0+10.58}$  is the central brightness of a pure disc ( $\mu_0 = 21.5 \pm 0.5$ , Bosma & Freeman 1993, Theureau et al. 1997). One expects then that  $m_{\text{lim}}$  increases slowly from early to late types with a total shift of 0.6 mag (value obtained with  $\log D_{\text{lim}} = 1.2$  and  $\mu_0 = 21.5$ , see Sect. 5).

### 2.3. 21-cm line measurements

All raw 21-cm line widths, collected from LEDA, have been reduced to a common system of widths at 20 % and 50 % of the peak (Bottinelli et al. 1990). They are corrected for velocity resolution effect and tested for homogeneity. Large part of the data (almost 50 %) is based on our own observations at the Nançay Radiotelescope. The detection rate at Nançay was excellent (roughly 90 %). The correction for internal velocity dispersion was made according to Tully & Fouqué (1985). Finally,

$$\log V_m = \langle (2 \cdot \log w_{20} + \log w_{50})/3 \rangle - \log (2 \sin(I)),$$

where  $I$  is the inclination of the galaxy. The uncertainties on  $\log V_m$  are typically around 0.08, as calculated according to Bottinelli et al. (1983).

### 2.4. Radial velocities and kinematical distances

Heliocentric radial velocities from optical or radio measurements are corrected to the centroid of the Local Group according to Yahil et al. (1977). The original optical compilation was

made for the preparation of the RC3 catalogue (Fouqué et al. 1992). Radio velocities come essentially from 21-cm line measurements; they have been homogenized and tested for scale, zero-point errors, and reference effect (Bottinelli et al. 1990).

Radial velocities are used to define a kinematical distance scale,  $d_{\text{kin}}$ , with an infall component in the direction of the Virgo Cluster ( $(l, b) = (284^\circ, 74^\circ)$ ). Similarly as in BGPT86, we applied Peebles's (1976) linear infall model. In most of the calculations we used  $(V_0)_{\text{vir}} = 980 \text{ km s}^{-1}$  (Mould et al. 1980) for the Virgo mean velocity and  $v_0 = 150 \text{ km s}^{-1}$  as in Bottinelli et al. (1995) for the LG infall.

### 2.5. Morphological types

Even after attempts to characterize rigorously the elements of the Hubble sequence, morphological type still remains a rather subjective datum, and experience shows that its definition depends on astronomer. We adopted the RC3 system as a standard, and converted to it the morphological types from other catalogues (see Paturel et al. 1997).

### 2.6. Adopted restrictions

The sample was restricted according to the following criteria:

- $|b| \geq 15^\circ$ , to exclude objects near the Galactic plane having poorly defined magnitudes; this concerns 420 galaxies of our sample
- $\log R_{25} \geq 0.07$  to exclude face-on galaxies for which the calculated  $\log V_m$  is uncertain. This concerns 501 galaxies of our sample
- galaxies belonging to the triple value region around the center of the Virgo cluster have been excluded (see BGPT86). This concerns 107 galaxies in the case of our standard velocity field
- very close galaxies (sometimes with negative radial velocity) are excluded because of the importance of their peculiar motions

After these restrictions, we are left with 4164 and 3622 galaxies for the diameter and magnitude TF relations, respectively.

## 3. The method of normalized distances

In BGPT86 the method of normalized distances, based on a discussion of the Malmquist bias in TF distance moduli (Teerikorpi 1984), was first applied to a sample of field galaxies. The method is based on the expectation that the mean Hubble ratio  $\langle H \rangle_p$  averaged over all galaxies at the same (kinematical) distance and with the same value of  $p = \log V_m$ , starts to increase at some limiting kinematical distance. Here the magnitude limit begins to cut away the faint part of the luminosity function  $\Phi(M)_p$ . For different  $\log V_m$  the limiting distance will be different by the factor  $10^{0.2a(p-p_0)}$  from the TF relation  $M = a \cdot p + b$ . Hence, if one multiplies  $d_{\text{kin}}$  by  $10^{-0.2a(p-p_0)}$ , the behaviour of  $\langle H \rangle_p$  will be the same along the thus derived normalized distance ( $d_n$ ) axis. Finally, one inspects the  $\langle \log H \rangle$  vs.  $d_n$  diagram for the unbiased

plateau seen at small normalized distances as a horizontal part, now for all  $\log V_m$  together.

The luminosity function  $\Phi(M)_p$  is supposed to be nearly gaussian, with a constant dispersion  $\sigma_{M_p}$  over all values of  $p$ . These assumptions are realistic in view of the distribution of absolute magnitudes for different  $\log V_m$  ranges. In some recent studies (Giovanelli 1996) it has been argued that  $\sigma_{M_p}$  is larger at smaller  $\log V_m$ . However, we did not find such a tendency in our plateau sample (cf. Fig. 1). The TF relation itself also shows a regular distribution of the points along the regression line, allowing us to consider  $\sigma_{M_p}$  equal to the intrinsic TF scatter, except perhaps for small galaxies where measurement errors in diameters become important. The method of normalized distances was discussed and verified in BGPT86, Bottinelli et al. (1988), Bottinelli et al. (1995), and also in Ekholm (1996) by using synthetic data sets.

### 3.1. Analytical description

In its original form, the formula for the normalized kinematical distance was essentially given as

$$d_n = d_{\text{kin}} 10^{0.2a(2.7 - \log V_m)} \quad (2)$$

(magnitude relation, BGPT86).

This expression is for the ideal case where the sample is complete up to a given apparent magnitude limit or down to a given apparent diameter limit. But we may desire to use data from several different catalogues, each being complete up to a different apparent limit. It is then necessary to introduce an additional term for the definition of the normalized distance:

$$d'_n = d_n 10^{0.2(m_0 - m_{\text{lim}})}, \quad (3)$$

where  $m_0$  may be arbitrarily chosen and  $m_{\text{lim}}$  depends on the catalogue. An example may be found in Bottinelli et al. (1988), where the study was done with different samples selected according to different  $\log V_m$  ranges.

The influence of the magnitude limit on the bias properties has been well illustrated also by Sandage (1994a) using the device of the Spaenhauer diagram. The importance of a well defined limit was further discussed by Federspiel et al. (1994) in their analysis of the Mathewson-Ford-Buchhorn sample. Consequently, using the type dependent TF relation, we have to pay attention to the fact that, the sample being diameter selected, the magnitude limit will be different from one type to another. Thus, the factor  $10^{0.2(m_0 - m_{\text{lim}}(T))}$  has to be used.

It is also important to note that galaxies of the same type and  $\log V_m$ , but of different inclinations form separate classes as far as the Malmquist bias is concerned. Highly inclined galaxies are much fainter in the sky than similar face-on galaxies at similar distance. Hence, they fall below the (magnitude) detection limit at a smaller distance than the face-on galaxies. In the same way, one must take into account the galactic extinction  $a_g$ : in regions behind an enhanced extinction, galaxies appear smaller and fainter than elsewhere, hence, their normalized distance is

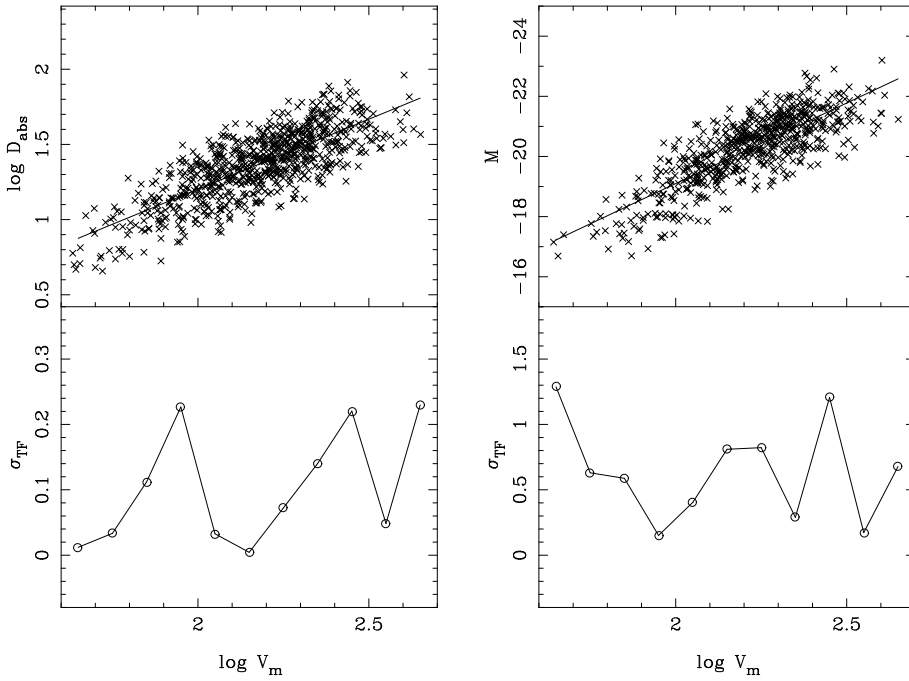


**Fig. 1.** Diameter (left) and magnitude (right) TF relations and their dispersions at different  $\log V_m$ .

larger. These effects were taken into account in Bottinelli et al. (1995), where the formula was written:

$$d_n = d_{\text{kin}} \cdot 10^{0.2a(\log V_m - 2.7)} \cdot 10^{0.2A(R)} \cdot 10^{0.2a_g} \cdot 10^{0.2(m_0 - m_{\text{lim}})}, \quad (4)$$

for magnitude relation, or

$$d_n = d_{\text{kin}} \cdot 10^{a(2.7 - \log V_m)} \cdot 10^{-C \log R} \cdot 10^{0.094a_g} \cdot 10^{(\log D_{\text{lim}} - \log D_0)}, \quad (5)$$

for diameter relation.

Here the factor  $A(R)$  or the constant  $C$  takes care of the influence of the inclination angle on the observed magnitude or diameter. However, this term practically vanishes when one uses the diameter relation:  $C = 0.04$  (Bottinelli et al. 1995).

Following the same idea, one must also take into account the fact that the zero-point  $b = b(T)$  of the TF relation depends strongly on morphological type  $T$  (Theureau et al. 1997). Using  $d_{n,T} = d_n 10^{0.2(b(6) - b(T))}$ , all galaxies are shifted to type  $T = 6$ , which was chosen as a reference because it is one of the better populated and shows the nicest TF regression.

### 3.2. On the Spaenhauer diagram method

One can but note the similarities that exist between our normalized distance method and the method based on the use of the Spaenhauer diagram (Sandage, 1988a, 1994a, 1994b, Federspiel et al., 1994). The philosophical basis and hypotheses are indeed approximately the same, even if the methods are formally different.

Both methods assert the importance of the Malmquist effect on the estimation of the Hubble constant when using a flux-limited sample. Both assert that the bias considered here depends on the distance (Teerikorpi 1975, 1984, Sandage 1994a)

and that the selection of an unbiased subsample is the only way to derive the good TF slope and an unbiased value of  $H_0$  from field galaxies. It is also clear that the bias depends on  $\log V_m$  (BGPT86, Bottinelli et al. 1988, Sandage 1994b), and consequently that the limit of the unbiased regime is a function of  $\log V_m$ . Moreover, it is shown that attempts to get the volume-limited (unbiased) subsample or to correct for the bias, require the strict completeness of the sample either in magnitude or in diameter, depending on the TF relation used (BGPT86, Federspiel et al. 1994). Hence, redshift,  $\log V_m$ , and magnitude limit, constituting the elements of Sandage's "triple-entry-correction", are also included in the method of normalized distance, in fact, in formulae (4) and (5). Note also that, both methods assume the symmetry of the luminosity function of a given class of objects (fixed  $\log V_m$ , given type) and its invariability with distance.

However, the two methods have also differences. Sandage's method is, in a certain way, more empirical: it consists of dividing the sample in discrete boxes of  $\log V_m$  to identify for each  $\log V_m$  range separately, the corresponding unbiased region. Our more analytical method allows to treat the  $\log V_m$  values continuously, all the objects being used in the same diagram to extract an optimal "plateau", statistically better defined due to the larger number of points. In addition, the normalized distance method permits one to take into account also more subtle effects due to inclination (i.e. opacity), galactic absorption, and morphological type or mean surface brightness. In addition, the normalized distance scale, the unbiased plateau, and the derived TF slope, are obtained by iteration and therefore optimized. Finally, the Spaenhauer method requires as assumption the uniformity of density to determine the unbiased subsample by fitting the estimated envelopes of the sample to the data plot. Our method

**Table 1.** Primary calibrator sample; galaxies with Cepheid distances. The values in columns 3–7 are taken from KLUN-sample or from LEDA database. Sources for the distance moduli are listed in column 8.

| Cepheid distances |       |                 |         |            |     |       |                         |
|-------------------|-------|-----------------|---------|------------|-----|-------|-------------------------|
| Name              | $\mu$ | $\log D_{25}^0$ | $B_T^0$ | $\log V_m$ | $T$ | $V_0$ | Source                  |
| N 224             | 24.42 | 3.19            | 3.25    | 2.397      | 3   | -14   | Freedman & Madore 1990  |
| N 300             | 26.66 | 2.34            | 8.44    | 1.912      | 7   | 124   | Freedman et al. 1992    |
| N 598             | 24.64 | 2.82            | 5.72    | 1.982      | 5   | 68    | Freedman et al. 1991    |
| N 925             | 29.84 | 2.07            | 9.72    | 2.008      | 7   | 782   | Silbermann et al. 1996a |
| N1365             | 31.36 | 2.05            | 9.82    | 2.305      | 3   | 1565  | Silbermann et al. 1996b |
| N2403             | 27.50 | 2.34            | 8.20    | 2.047      | 6   | 299   | Freedman & Madore 1988  |
| N3031             | 27.80 | 2.34            | 7.10    | 2.333      | 2   | 123   | Freedman et al. 1994b   |
| N3368             | 30.32 | 1.89            | 9.51    | 2.312      | 2   | 760   | Tanvir et al. 1995      |
| N3621             | 28.95 | 2.12            | 9.07    | 2.151      | 7   | 436   | Rawson et al. 1996      |
| N3627             | 30.37 | 1.90            | 8.99    | 2.241      | 3   | 596   | Tanvir et al. 1995      |
| N4321             | 31.15 | 1.87            | 9.73    | 2.269      | 4   | 1481  | Freedman et al. 1994a   |
| N4496A            | 31.13 | 1.57            | 11.82   | 1.994      | 6   | 894   | Saha et al. 1996a       |
| N4536             | 31.10 | 1.85            | 10.28   | 2.198      | 4   | 1640  | Saha et al. 1996b       |
| N4639             | 32.00 | 1.48            | 11.62   | 2.270      | 4   | 894   | Sandage et al. 1996     |
| N5253             | 28.01 | 1.60            | 9.86    | 1.541      | 2   | 155   | Saha et al. 1995        |

does not need such a strong hypothesis to fix confidently the limit of the plateau.

#### 4. Primary calibrator galaxies

In order to determine the absolute zero-points for the TF relations, and consequently, the absolute distance scale and the value of  $H_0$ , one needs a sample of calibrators. Furthermore, this sample should be statistically equivalent to a volume-limited sample, providing unbiased  $\langle M \rangle_p$  or  $\langle \log D \rangle_p$ . The galaxies which can be used to build such a sample come from rather heterogeneous observational programmes, with different distance indicators applied, and not always collected with the requirement of volume-limitedness in mind.

##### 4.1. Galaxies with Cepheid distances

The number of galaxies with Cepheid distances is increasing rapidly. The on-going Hubble Space Telescope programmes (cf. Kennicutt et al. 1995, and Sandage et al. 1996) aim at measuring Cepheids in 25 galaxies. 18 of these galaxies have been chosen as optimal calibrators for the IR Tully-Fisher relation. Together with Cepheid observations with advanced ground-based telescopes (e.g. Pierce et al. 1994) we now have a larger sample of calibrator galaxies with more accurate distances than in BGPT86. The range of distances has increased considerably; the first Cepheids in Virgo galaxies have been successfully detected.

We have collected all the galaxies with Cepheid distances and excluded face-on ones, and those being very peculiar or outside the type range  $T = 1 - 8$ .

Though we excluded the low inclination galaxies N4571 and N5457 (=M101), distance to M101 was used for its close companions (cf. Table 2). The very peculiar ‘‘Sombrero’’ galaxy (M104) was excluded together with several galaxies of irregular types  $T = 9-10$  (I10, I4182, I1613, N6822, Sex A, Sex B).

**Table 2.** Secondary calibrator sample; galaxies with group distances. Distances to Sculptor Group galaxies are determined from the Cepheid distance to group member N300 and from resolution arguments (Tammann 1987). M81 Group distance is defined as intermediate between two group members N3031 (=M81) and N2403. Cepheid distance of  $\mu = 29.34$  to N5457 (=M101) has been recently measured with HST (Kelson et al. 1996), but being a face-on galaxy, it was not included in our primary calibrators. Leo Group distance is adopted from the member galaxy N3368.

| Group distances |       |                 |         |            |     |       |
|-----------------|-------|-----------------|---------|------------|-----|-------|
| Name            | $\mu$ | $\log D_{25}^0$ | $B_T^0$ | $\log V_m$ | $T$ | $V_0$ |
| Sculptor Group  |       |                 |         |            |     |       |
| N 247           | 26.80 | 2.21            | 8.80    | 1.976      | 7   | 231   |
| N 253           | 27.50 | 2.29            | 7.00    | 2.277      | 5   | 298   |
| N7793           | 27.50 | 1.98            | 9.33    | 1.985      | 7   | 253   |
| N1023 Group     |       |                 |         |            |     |       |
| N 891           | 29.80 | 2.14            | 9.38    | 2.325      | 3   | 776   |
| N1003           | 29.80 | 1.79            | 10.66   | 1.980      | 6   | 863   |
| Fornax Group    |       |                 |         |            |     |       |
| N1350           | 31.36 | 1.74            | 13.38   | 2.377      | 2   | 1805  |
| M81 Group       |       |                 |         |            |     |       |
| N2976           | 27.65 | 1.74            | 10.14   | 1.731      | 5   | 159   |
| N4236           | 27.65 | 2.26            | 9.08    | 1.834      | 8   | 164   |
| Leo Group       |       |                 |         |            |     |       |
| N3299           | 30.32 | 1.29            | 13.51   | 1.838      | 8   | 509   |
| N3351           | 30.32 | 1.87            | 9.89    | 2.183      | 3   | 641   |
| N3627 Group     |       |                 |         |            |     |       |
| N3628           | 30.37 | 2.11            | 9.20    | 2.329      | 3   | 597   |
| N3623           | 30.37 | 1.95            | 9.33    | 2.354      | 1   | 677   |
| M101 Group      |       |                 |         |            |     |       |
| N5204           | 29.34 | 1.67            | 11.16   | 1.719      | 8   | 332   |
| N5477           | 29.34 | 1.21            | 14.04   | 1.523      | 8   | 427   |
| N5585           | 29.34 | 1.74            | 10.81   | 1.878      | 7   | 442   |

**Table 3.** A list of Hubble Space Telescope extragalactic distance scale project galaxies. As the project continues, the reader may fill the gaps and add these galaxies in the primary calibrators. Following methods explained in the text, the TF relations may then be re-calibrated and value of  $H_0$  re-evaluated.

| More HST Key Project galaxies |                     |                 |         |            |     |       |
|-------------------------------|---------------------|-----------------|---------|------------|-----|-------|
| Name                          | $\mu$               | $\log D_{25}^0$ | $B_T^0$ | $\log V_m$ | $T$ | $V_0$ |
| N1425                         |                     | 1.78            | 10.62   | 2.242      | 3   | 1440  |
| N2090                         |                     | 1.75            | 10.96   | 2.149      | 5   | 755   |
| N2541                         |                     | 1.81            | 11.14   | 1.962      | 6   | 647   |
| N3198                         |                     | 1.92            | 9.86    | 2.162      | 5   | 703   |
| N3319                         |                     | 1.79            | 10.89   | 2.010      | 6   | 763   |
| N3351                         | cf. Leo Group above |                 |         |            |     |       |
| N3521                         |                     | 2.05            | 9.01    | 2.356      | 4   | 614   |
| N4414                         |                     | 1.59            | 10.35   | 2.326      | 5   | 694   |
| N4535                         |                     | 1.86            | 10.11   | 2.231      | 5   | 1822  |
| N4548                         |                     | 1.72            | 10.60   | 2.255      | 3   | 379   |
| N4725                         |                     | 2.03            | 9.57    | 2.389      | 2   | 1160  |
| N7331                         |                     | 2.04            | 9.15    | 2.388      | 3   | 1115  |

We are left with 15 galaxies for our primary calibrator sample. In Table 1, the Cepheid distances, corrected apparent diameters and  $B$ -magnitudes, rotational velocities, types, and radial velocities ( $V_0$ ), of these galaxies are listed. Sources for distances are given, other values are from our KLUN-sample or from LEDA.

In Table 2 we list possible members of groups with distances known from primary calibrators. For these we attach the mean group distance, except in the case of Sculptor group, where the distance differences are defined from resolution into brightest stars (Tammann, 1987). The 15 galaxies in Table 2 form our secondary calibrator sample. Combining these with the primary sample we enlarge the number of calibrators, which increases statistical reliability even though the distances in Table 2 are obviously not as accurate as in the primary sample. All the types 1–8 are represented in the combined sample.

For the convenience of the reader we list in Table 3 the rest of the Hubble Space Telescope Key Project galaxies. As the project continues, these galaxies may easily be added to the previous calibrator list. In the Appendix, we derive an algorithm for re-evaluating the value of  $H_0$  with the more complete calibrator sample.

#### 4.2. BGPT86 calibrators

The calibrators used in BGPT86 had distances from several different methods — Cepheids, brightest stars, H II regions, luminosity indices, novae, etc. In the present work we use only Cepheid distances, which are now sufficiently numerous and rest on a firm physical and observational basis.

Nine of the BGPT86 calibrators with new distances are found in Tables 1 and 2. Only the Magellanic Clouds, being of irregular type, have been dropped out. Ten years ago we used three different sets of distances: de Vaucouleurs scale, and “old” and “new” Sandage and Tammann scales (Table 4 in BGPT86). On average the distance moduli of the deV-scale were smaller

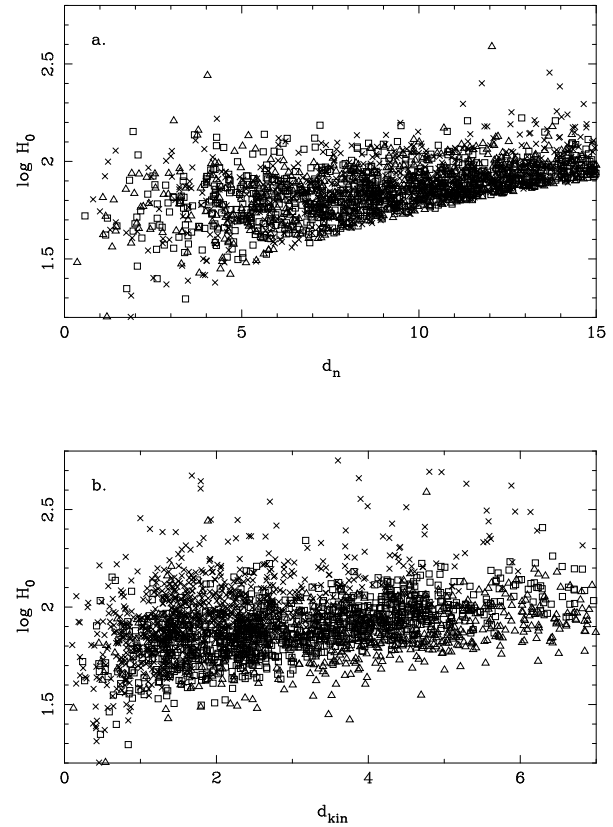


**Fig. 2.** Plateau diagrams for the diameter relation. In **a.**, the values of  $\log H_0$  for individual galaxies are plotted against normalized distance, in **b.** the kinematical distances are used. The different  $\log V_m$ -ranges are denoted with:  $\times$  for  $\log V_m \leq 2.1$ ,  $\square$  for  $2.1 < \log V_m < 2.3$ , and  $\triangle$  for  $\log V_m \geq 2.3$ .

by  $\langle \Delta \mu \rangle = 0.22$ , “old” and “new” ST-scales were larger than the present values,  $\langle \Delta \mu \rangle = -0.33$  and  $-0.06$  respectively.

In terms of the Hubble constant, deV-scale gives  $H_0$  that is 11% larger, “old” and “new” ST-scales give values of  $H_0$  that are 14% and 3% smaller than when the present distances are used.

#### 5. Unbiased TF parameters

In the method of normalized distances, unbiased TF parameters are derived by selecting an unbiased subsample on the basis of a  $\log H$  vs.  $d_n$  diagram. This iterative way requires as input a reasonable value of the TF slope  $a$  (we used the values of  $a$  and  $b$  given by Bottinelli et al. 1995 and Fouqué et al. 1990:  $a_D = 0.9$ ,  $b_D = -1.0$ ,  $a_M = -5.5$ ,  $b_M = -8.0$ ).  $\log H$  is calculated for each galaxy as the logarithm of the ratio of the corrected radial velocity  $V_c$  and TF distance  $d_{TF}$  (in Mpc), where:

$$d_{TF} = 10^{(m - a_M \log V_m - b_M - 25)/5}$$

for the magnitude relation, or

$$d_{TF} = 10^{(a_D \log V_m + b_D - \log D_{25})}$$

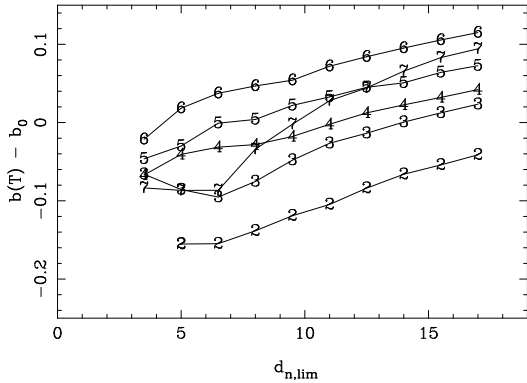


**Fig. 3.** Relative diameter TF zero-points for different types and different plateau-limits ( $d_{n,\text{lim}}$ ). Early types  $T = 1$  and 2 are combined and marked with number 2. Late types  $T = 7 - 8$  are similarly marked with 7.

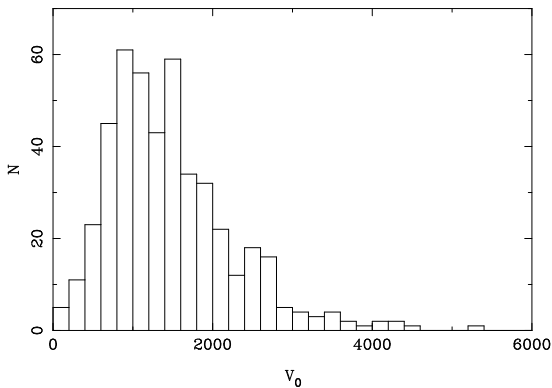


**Fig. 4.** Distribution of plateau galaxies with respect to radial velocity  $V_0$ . The number of galaxies in the diameter TF unbiased plateau is 478.

for the diameter relation. At each step, an unbiased subsample consisting of galaxies located in the horizontal part of the plot (the plateau) is extracted, and new TF parameters are evaluated by a least square regression of  $\log D$  or  $M$  against  $\log V_m$ .  $\log D$  and  $M$  are calculated using the kinematical distance  $d_{\text{kin}}$  (cf. Sect. 2.4.), and the apparent diameter  $D_{25}$  or the apparent  $B$ -magnitude  $B_1^0$  respectively.

One may ask how sensitive the results of the normalized distance method are either to the choice of the velocity infall model or to the random galaxy peculiar motions. And do we, in the ideal case of a perfectly known velocity field, actually get the true TF parameters. Such questions were studied by Ekholm (1996) using Monte-Carlo simulations. We summarize here some of his results:

1. The inferred TF *slope* does not depend critically on the precise knowledge of the unbiased plateau.
2. The unbiased plateau and the derived slope are quite insensitive to the adopted value of the infall velocity of the Local Group toward Virgo.

3. The linearized model of Peebles (1976), that we use to define the kinematical distance scale (Sect. 2.4), seems to be an excellent approximation in the case of the underlying Tolman-Bondi flow, when a very accurate value of the Local Group infall velocity is not needed.
4. Velocity dispersions lower than  $100 \text{ km s}^{-1}$  do not affect the above conclusions. In the literature, a value of  $\sigma_V = 80 - 90 \text{ km s}^{-1}$  is generally accepted (Faber & Burstein 1988), and even smaller ones have been advocated (Sandage 1994b).

### 5.1. Direct diameter TF relation

We apply the method of normalized distances first to the diameter TF relation. In Fig. 2, individual  $\log H$  values are plotted both against the kinematical distance scale and the normalized distance scale, to illustrate the effect of the normalization on the putative plateau. Three ranges of  $\log V_m$  values are represented with different icons: crosses correspond to  $\log V_m$  in  $[1.3, 2.1]$ , open squares to  $\log V_m$  in  $]2.1, 2.3[$ , and open triangles to  $\log V_m$  in  $[2.3, 2.8]$ . These intervals contain respectively 949, 967 and 686 objects. According to Sect. 3, objects with small values of  $\log V_m$  are expected to be biased at smaller distances than those with larger values. This is well seen in the kinematical distance diagram (Fig. 2a): Though well mixed at small distances (all  $\log V_m$  ranges are consistent with a same mean value  $\langle \log H \rangle$ ), galaxies with small  $\log V_m$  (crosses) appear rapidly in the upper part of the diagram as the distance increases. For galaxies with large values of  $\log V_m$  (open triangles),  $\langle \log H \rangle$  stays longer around the unbiased constant value. In the normalized distance diagram, all the galaxies follow the same behaviour: their mean value  $\langle \log H \rangle$  begins to go up at some common  $d_n$ . The plateau region appears then very clearly in the low  $d_n$  range ( $d_n \leq 6$ ).

Fig. 3 shows the derived type dependent zero-points against increasing normalized distance limit; each set of zero-points corresponds to a subsample defined by  $d_n \leq d_{n,\text{lim}}$ . Types 1 and 2, and types 7 and 8 have been grouped together for convenience, the number of points in these types being separately not large enough to show well the zero-point differences. The reader may see again the effect of the bias which appears for  $d_{n,\text{lim}} > 6$  and leads to an overestimation of the zero-points. However, the relative positions of the different  $b(T)$  ( $T=1$  to 8) do not vary much with increasing  $d_n$  limit, and moreover, the increasing number of points available makes the relative shift much more evident. If needed, this gives additional support to the reality of the type effect for the direct relation.

Our final adopted unbiased plateau ( $d_{n,\text{lim}} = 6$ ) contains 478 points, distributed in radial velocity  $V_0$  as shown by Fig. 4.

Table 4 presents a summary of our results on TF parameters. Again, types 1 – 2 and 7 – 8 have been grouped together. In column 2, the adopted TF slope  $\langle a \rangle$  is given; it corresponds to a weighted mean over the slopes derived for each type. In columns 3 and 4 the adopted type dependent TF zero points are listed:  $b(T)_1$  and  $b(T)_2$  refer to the calibrator sample used; our primary Cepheid calibrator sample, and our extended ‘‘Cepheid + group membership sample’’ respectively (Tables 1 and 2). Column 5 gives the number of objects.

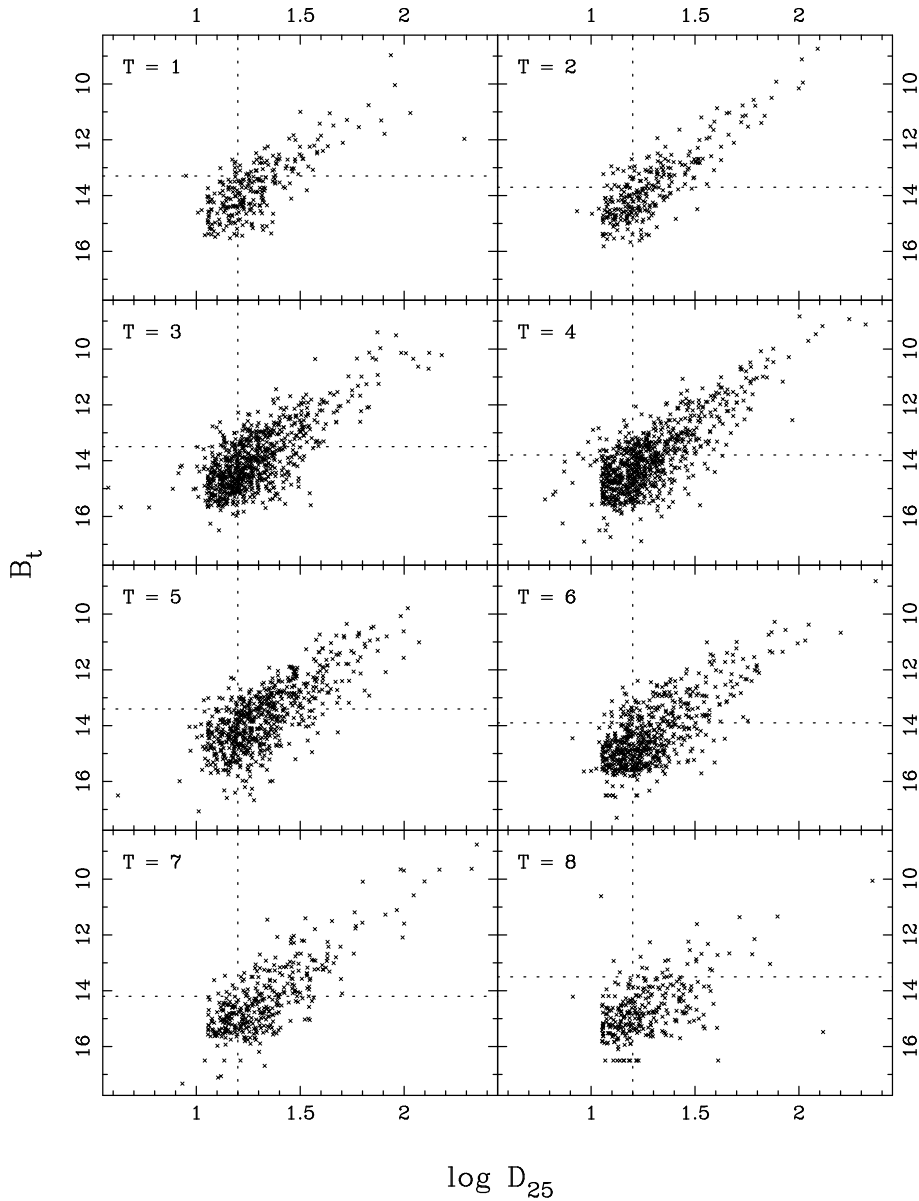


**Fig. 5.**  $\log D_{25} - B_t$  diagrams for different morphological types. From these diagrams the type dependent magnitude completeness limits may be estimated. We adopted the following values:  $m_{\text{lim}}(1) = 13.3$ ,  $m_{\text{lim}}(2) = 13.7$ ,  $m_{\text{lim}}(3) = 13.5$ ,  $m_{\text{lim}}(4) = 13.8$ ,  $m_{\text{lim}}(5) = 13.4$ ,  $m_{\text{lim}}(6) = 13.9$ ,  $m_{\text{lim}}(7) = 14.2$ ,  $m_{\text{lim}}(8) = 13.5$ . Dashed lines show these limits and the diameter completeness limit ( $\log D_{25,\text{lim}} = 1.2$ ).

**Table 4.** See text for details.

| Diameter TF parameters |                     |          |          |     |
|------------------------|---------------------|----------|----------|-----|
| $T$                    | $\langle a \rangle$ | $b(T)_1$ | $b(T)_2$ | $n$ |
| 1,2                    |                     | -1.028   | -1.063   | 58  |
| 3                      |                     | -0.956   | -0.991   | 79  |
| 4                      | 1.082               | -0.905   | -0.940   | 104 |
| 5                      |                     | -0.880   | -0.915   | 103 |
| 6                      |                     | -0.847   | -0.882   | 81  |
| 7,8                    |                     | -0.968   | -1.003   | 53  |

The relative zero-points  $b(T) - b(6)$  were calculated using the field galaxies (plateau data), whereas the absolute values were fixed with the calibrators: knowing the relative trend, calibrators are normalized to type 6 and, forcing the slope to the weighted mean value  $\langle a \rangle$ , an absolute zero-point  $b_c(6)$  is calculated (see also the Appendix).

## 5.2. Direct magnitude TF relation

Fig. 6 illustrate again the effect of distance normalization, now using the magnitude TF relation. We took into account the variation of  $m_{\text{lim}}$  with the morphological type. The unbiased plateau is slightly better determined and contains more points using the normalization on  $m_{\text{lim}}(T)$  rather than a common brighter cut-off at  $m_{\text{lim}} = 13.25$  mag. Here, we used the values of  $m_{\text{lim}}(T)$  derived from the sample itself, with the help of apparent magnitude histograms or  $\log D_{25}$  vs.  $B_t$  diagrams (Fig. 5). Fig. 7 shows the values observed for each type, together with the predicted ones as given by Eq. (1) in Sect. 2.2. Even if the plot is rather noisy, the data appear consistent with a general increase of  $m_{\text{lim}}$  with increasing type code  $T$ . It is also clear that the predicted values (open circles) cannot be used: they just illustrate a general behaviour of  $m_{\text{lim}}$  with increasing  $T$ . In fact, the model is very sensitive to any change in the value of its param-

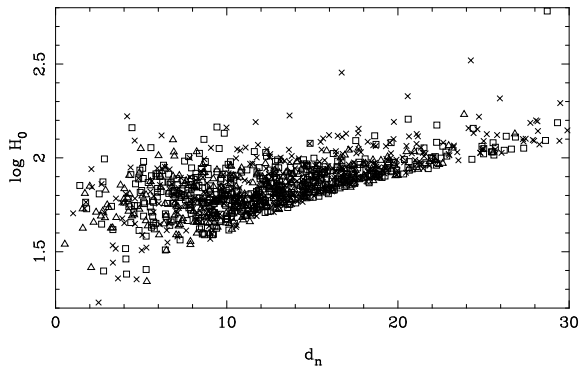


**Fig. 6.** Plateau diagram for the magnitude relation. Different  $\log V_m$ -ranges are denoted similarly as in Fig. 2. Type dependent magnitude cutoff limits have been used.

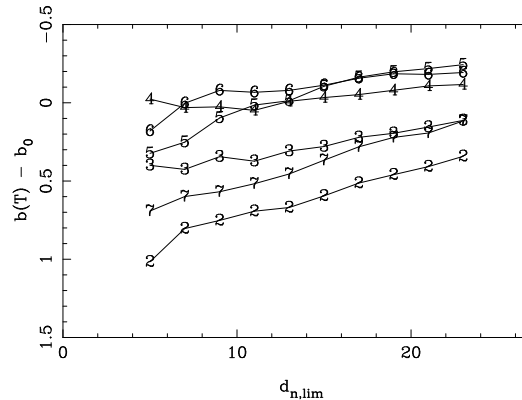


**Fig. 8.** Relative magnitude TF zero-points for different types and different plateau limits (cf. Fig. 3).

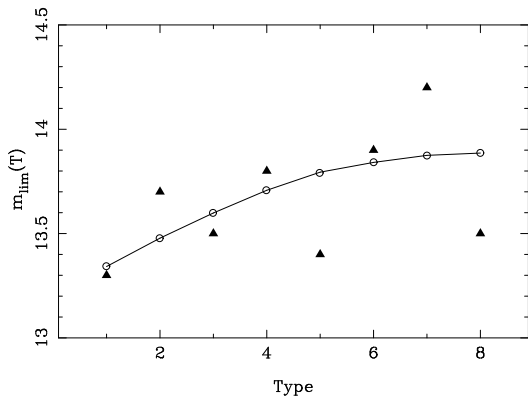


**Fig. 7.** The observed type dependent magnitude limits from Fig. 5 (triangles) and the corresponding values given by Eq. (1) (circles).

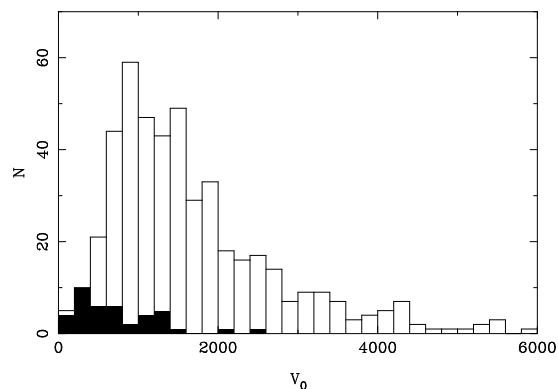
eters, and especially the value used for  $\mu_0$ : a constant central surface brightness is assumed for the disc, whatever the type is, which may be unrealistic. Sdm galaxies ( $T = 8$ ), for example, which appear clearly outside the global trend, are known to have a much lower surface brightness than other types. Hence, we assume that the observed variations are real, and adopt the empirical  $m_{\text{lim}}(T)$ .

Fig. 8 shows again the behaviour of the relative zero-points  $b(T) - b(6)$  with increasing  $d_{n,\text{lim}}$ . The plot is similar to what we obtained with diameters, but as expected from Theureau et al. (1997), the type effect is less clear.

The unbiased plateau ( $d_n \leq 10$ ) now contains 468 galaxies. In comparison, BGPT86 had only 40 plateau objects available. The  $V_0$ -distributions of our new and BGPT86 plateau samples are shown in Fig. 9.

The parameters of the magnitude relation were derived in the same way as with the diameter relation above. They are presented in Table 5.

One may ask why, with a smaller sample, we get in the plateau approximately the same number of points as in the diameter approach. This is caused by the smaller scatter in the magnitude TF relation which makes the plateau deeper.



**Fig. 9.** Distribution of plateau galaxies with respect to  $V_0$  (cf. Fig. 4). Number of galaxies in magnitude plateau is 468. For comparison we have added the 40 BGPT86 plateau galaxies in the same diagram.

**Table 5.**

| Magnitude TF parameters |                     |          |          |     |
|-------------------------|---------------------|----------|----------|-----|
| $T$                     | $\langle a \rangle$ | $b(T)_1$ | $b(T)_2$ | $n$ |
| 1,2                     |                     | -7.347   | -7.023   | 59  |
| 3                       |                     | -7.725   | -7.399   | 81  |
| 4                       | -5.823              | -8.001   | -7.675   | 111 |
| 5                       |                     | -8.034   | -7.710   | 72  |
| 6                       |                     | -8.109   | -7.784   | 82  |
| 7,8                     |                     | -7.499   | -7.174   | 63  |

## 6. The value of $H_0$

### 6.1. On the unbiased plateau

Strictly speaking, the method of normalized distances presupposes that the dispersion  $\sigma_{M_p}$ , arising from the intrinsic scatter and measurement errors, may be regarded as constant. Then the expected bias curves  $\langle \log H \rangle$  vs.  $d_{\text{kin}}$ , corresponding to different observed values of  $p$  ( $= \log V_m$ ), will be simply shifted along the  $d_{\text{kin}}$ -axis according to the factors appearing in the definition of the normalized distance, and come one over the other.

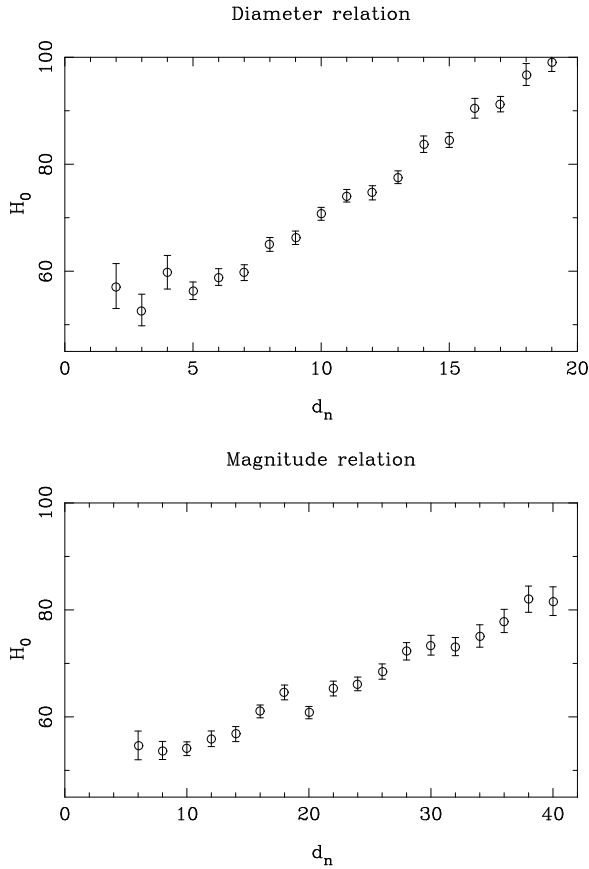


**Fig. 10.** The mean values of  $H_0$  (from  $\langle \log H_0 \rangle$ ) vs. normalized distance for diameter and magnitude TF relations.

Assuming gaussian distribution for the volume-limited  $M_p = M(p)$  and a constant  $\sigma_{M_p}$ , one can calculate theoretical expectations for  $\langle \log H \rangle$  vs.  $d_n$  in terms of error function (Teerikorpi, 1975; Bottinelli et al. 1988), revealing the horizontal unbiased plateau. These predictions do not depend on any assumption on the spatial distribution of galaxies, though they naturally require  $d_{\text{kin}}$ , from a kinematical model giving at least relative distances.

If one adds into the model a spiral galaxy space density distribution law, it is possible to see how well populated the unbiased plateau is. We define the plateau by the requirement that the cumulative average error  $\langle \Delta \log H_0 \rangle$  is less than some  $\varepsilon$  below the limiting  $d_n = d_n(\varepsilon)$ .

For instance, assuming homogeneous galaxy distribution and gaussian galaxy luminosity function (and a gaussian intrinsic dispersion  $\sigma_{M_p}$  for the TF relation), we have

$$\langle \Delta \log H_0 \rangle_{\text{cum}} = 0.2 \cdot \sqrt{2/\pi} \cdot \sigma_{M_p} \cdot \frac{\int_0^d \exp(-A^2) r^2 dr}{\int_0^d [1 - \text{erf}(A)] r^2 dr}$$

and

$$N/N_{\text{tot}} = \frac{\int_0^d [1 - \text{erf}(A)] r^2 dr}{\int_0^\infty [1 - \text{erf}(A)] r^2 dr}$$

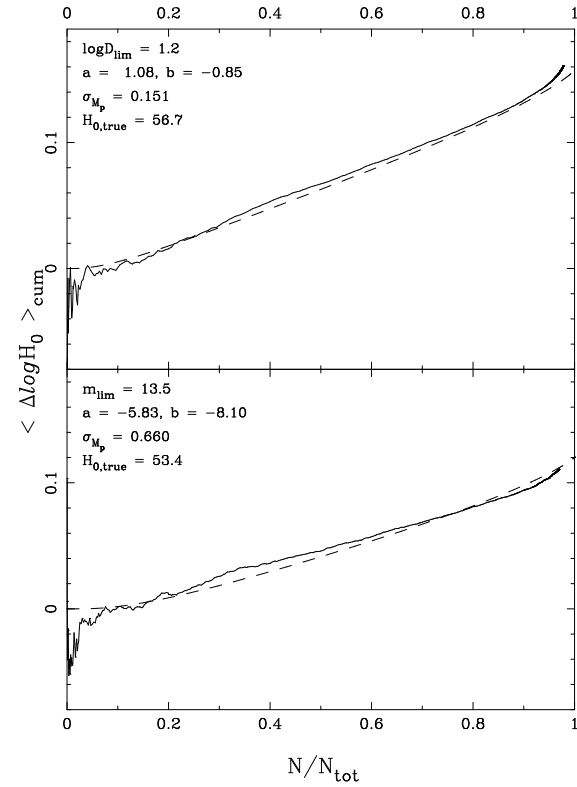


**Fig. 11.** Cumulative error of  $\langle \log H \rangle$  for different relative number of galaxies used for the plateau. The dashed line is from theoretical, the continuous line from observational values. Diameter relation is used in the top, magnitude relation in the bottom. The values of completeness limits, TF parameters and true  $H_0$  used for the theoretical curves are listed in both panels.

where  $A = (M_{\text{lim}}(r) - M_0)/(\sigma_{M_p} \sqrt{2})$ ,  $M_{\text{lim}}(r) = m_{\text{lim}} - 5 \log r - 25$ , and  $N/N_{\text{tot}}$  is the fraction of galaxies in the plateau. These formulae are connected by the distance  $d$  appearing as integration limit.

In the next subsection we use this expected run of  $\langle \Delta \log H_0 \rangle$  vs. the sample fraction  $N/N_{\text{tot}}$ , comparing it to the real data (Fig. 11). Typically, requiring that the error in  $\log H$  be less than 0.01, one should not accept the plateau to include more than about 10 per cent of the sample. Such curves are a useful tool when one tries to decide where it would be realistic to cut the plateau. Similar formulae may be derived using the diameter relation.

## 6.2. Results

In Fig. 10, mean values of  $\log H_0$  are shown against normalized distance  $d_n$ , both using the diameter and the magnitude TF relations. The effect of the Malmquist bias is clearly seen when objects are selected above  $d_{n,\text{lim}}$  where  $\langle \log H \rangle$  begins to grow quickly.

In Fig. 11, we have plotted both the observed and the theoretical curves corresponding to the cumulative average error  $\langle \Delta \log H_0 \rangle$ , as a function of the fraction of objects  $N/N_{\text{tot}}$  ac-

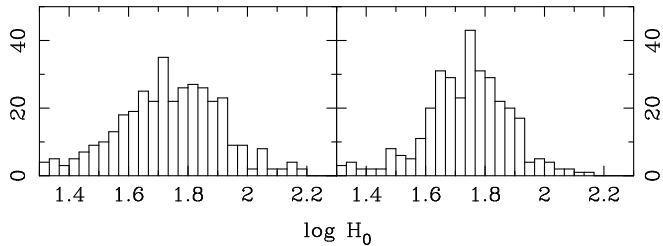


**Fig. 12.** Plateau  $\log H_0$  distributions for both relations, diameter on the left, magnitude on the right.

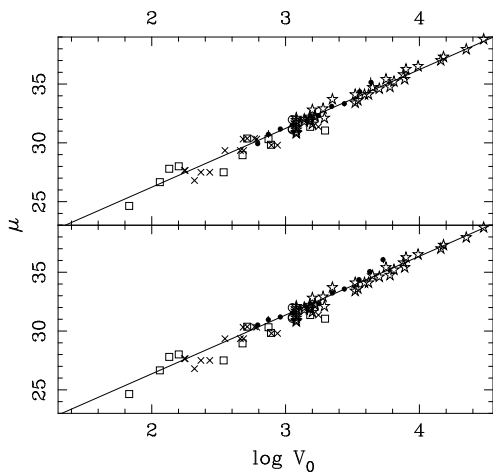


**Fig. 13.** Hubble diagrams. See text for details.

cepted to define our unbiased subsample. For a given scatter of the TF relation, we are able to decide which fraction of the sample we are allowed to keep in the unbiased plateau subsample. Even if the small number of points at short distances makes it noisy, the observed curve (full line) follows the predicted one (dashed line) quite well. The diagram suggests that we may not use more than 9 % and 12 % of our diameter-limited and our magnitude-limited samples, respectively. In practice this means that we may accept roughly 400 objects from each sample.

One also sees from these figures that the bias increases with a much slower rate when one uses the magnitude TF relation rather than the diameter TF relation. This is a direct consequence of the smaller scatter in the magnitude TF relation.

It is important to pay attention to the bad influence of the closest objects: large relative peculiar motions increase the dispersion and  $H_0$  is then poorly determined for small values of  $d_n$ . Moreover, the existence of a bulk flow such as the Local Anomaly (  $360 \text{ km s}^{-1}$  toward  $(l, b) = (199^\circ, 0^\circ)$  from Faber & Burstein, 1988) is expected to perturb the derived  $H_0$  value, making it smaller. For that reason, we excluded the galaxies within  $700 \text{ km s}^{-1}$  around the Local Group from our calculations, about 60 objects in total.

Table 6 summarizes our results for different plateau limits and the two calibrator samples presented in Tables 1 and 2. For the most relevant value of  $H_0$ , we adopted the unbi-

**Table 6.** Values for  $H_0$  with different plateau limits,  $H_{0,1}$  using Cepheid distance calibrators (Table 1) only,  $H_{0,2}$  with group distances (Table 2) also.

| Diameter TF relation  |                      |                      |      |
|-----------------------|----------------------|----------------------|------|
| $d_{n,lim}$           | $H_{0,1} \pm \sigma$ | $H_{0,2} \pm \sigma$ | n    |
| 3                     | $52.8 \pm 5.4$       | $57.2 \pm 5.1$       | 44   |
| 4                     | $54.6 \pm 5.2$       | $59.2 \pm 4.7$       | 105  |
| 5                     | $56.2 \pm 5.0$       | $60.9 \pm 4.4$       | 235  |
| 6                     | $56.7 \pm 4.9$       | $61.5 \pm 4.2$       | 403  |
| 7                     | $57.3 \pm 4.9$       | $62.1 \pm 4.2$       | 578  |
| 8                     | $58.7 \pm 5.0$       | $63.6 \pm 4.3$       | 782  |
| 9                     | $60.2 \pm 5.1$       | $65.2 \pm 4.3$       | 1032 |
| Magnitude TF relation |                      |                      |      |
| 5                     | $48.2 \pm 5.4$       | $55.8 \pm 5.7$       | 40   |
| 7                     | $52.2 \pm 5.3$       | $60.5 \pm 5.4$       | 114  |
| 9                     | $53.0 \pm 5.1$       | $61.4 \pm 5.2$       | 247  |
| 11                    | $53.4 \pm 5.0$       | $61.9 \pm 5.1$       | 415  |
| 13                    | $54.2 \pm 5.0$       | $62.8 \pm 5.1$       | 597  |
| 15                    | $54.8 \pm 5.1$       | $63.4 \pm 5.1$       | 780  |
| 17                    | $56.1 \pm 5.2$       | $65.0 \pm 5.2$       | 1010 |

ased subsamples defined as follows:  $d_{n,lim} \leq 6$  for the diameter relation and  $d_{n,lim} \leq 11$  for the magnitude relation. These give  $H_0 = 56.7 \pm 4.9 \text{ km s}^{-1} \text{ Mpc}^{-1}$  and  $H_0 = 53.4 \pm 5.0 \text{ km s}^{-1} \text{ Mpc}^{-1}$ , where the average has been calculated using 403 and 415 galaxies for the diameter and the magnitude relations respectively.

When calculating this average, we suppose the distribution of  $\log H = \log V_c - \log d_{TF}$  to be gaussian around a certain mean value, reflecting mostly the TF scatter. Fig. 12 shows the distribution of  $\log H$  for the diameter and the magnitude relations. Without galaxies belonging to the Local Anomaly, the observed shape of the distribution is obviously not far from gaussian.

To complete this section, we present in Fig. 13 Hubble diagrams for different kinds of samples: open squares and circles represent the objects in the pure Cepheid calibrator sample (the latter denoting Virgo galaxies), crosses represent the “group member” calibrators from Table 2, filled circles are the mean points obtained from our unbiased plateau of field galaxies, and finally we have also plotted as stars the SNIa standard candles of Sandage et al. (1996, see Sect. 7.4) which extend the diagram to large distances. Again, the diameter TF relation is used in the top and magnitude relation in the bottom panel. These different samples are in good agreement.

## 7. Discussion and conclusions

In this section we shall now discuss the legitimacy of our derived  $H_0$  value:  $H_0 = 56.7$  or  $H_0 = 53.4$  according to diameter or magnitude relation respectively. We study the influence of the velocity field model used to define the kinematical distance scale, comment on the adopted galactic absorption, and discuss the choice of the calibrator sample. We finally compare our results to those of the supernova method reaching larger redshifts.

**Table 7.** Values for  $H_0$  with different LG Virgo infall and observed Virgo recession velocities.

| $v_0$ | $(V_0)_{\text{Vir}}$ | Used in                    | $H_0$ (diam)   | $H_0$ (mag)    |
|-------|----------------------|----------------------------|----------------|----------------|
| 150   | 980                  | This paper                 | $56.7 \pm 4.9$ | $53.4 \pm 5.0$ |
| 185   | 980                  | This paper <sup>1</sup>    | $56.4 \pm 4.9$ | $53.4 \pm 5.2$ |
| 225   | 980                  | This paper <sup>1</sup>    | $59.2 \pm 5.0$ | $55.0 \pm 5.0$ |
| 220   | 950                  | Tammann et al. (1996)      | $59.1 \pm 5.0$ | $54.9 \pm 5.1$ |
| 331   | 1073                 | Huchra (1986) <sup>2</sup> | $59.8 \pm 4.8$ | $54.3 \pm 5.4$ |
| 372   | 1225                 | Huchra (1986) <sup>3</sup> | $57.4 \pm 4.9$ | $53.6 \pm 5.6$ |
| 290   | 937                  | Huchra (1986) <sup>4</sup> | $60.6 \pm 5.3$ | $55.9 \pm 5.4$ |

1. cf. Sect. 7.1.2

2. preferred values

3. “highest estimate”

4. “lowest estimate”

### 7.1. Influence of the velocity field model

We have used a linear velocity model (Peebles 1976) with  $v_0$  = Local Group infall velocity toward Virgo =  $150 \text{ km s}^{-1}$  and  $(V_0)_{\text{Vir}}$  = observed Virgo radial velocity =  $980 \text{ km s}^{-1}$ . As noted in Sect. 5, the linear Peebles’s model is a good approximation of the non-linear or Tolman-Bondi solution (e.g. Kraan-Korteweg, 1986) outside the triple-value region.

Particularly in the methods which use directly the Virgo cluster, changing the velocity model has a crucial effect on the derived  $H_0$ . In Table 7 we list our values of  $H_0$  obtained when different velocity parameters are used. The choice of  $v_0$  and  $(V_0)_{\text{Vir}}$  do not seem to affect significantly the results, all models are compatible with  $H_0 = 57 \pm 4 \text{ km s}^{-1}$ .

Some understanding on the small sensitivity of  $H_0$  is provided by numerical experiments. We tested how accurately the Peebles model gives kinematical distances and individual  $H_0$  values when we assume an underlying exact Tolman-Bondi velocity field and use somewhat erroneous value for the Local Group infall velocity.

#### 7.1.1. Sensitivity to errors in the model

We conducted a theoretical experiment asking how large an error emerges in the kinematical distances if the adopted value for  $v_0$  is larger (smaller) than the “true” value. Results from this experiment are shown in Fig. 14.

A uniform  $100 \times 100$  grid was created. We assume the true distance  $d_t$  in Virgo units and the angular distance  $\Theta$  with respect to Virgo to be known for each grid point. For each  $(d_t, \cos \Theta)$ -pair the corresponding observed velocity  $V_0$  is calculated from the Tolman-Bondi solution. For details of the model cf. Ekholm (1996). Two possibilities were considered: either  $v_0 = 100 \text{ km s}^{-1}$  or  $v_0 = 200 \text{ km s}^{-1}$ . The common parameters used were  $q_0 = 0.5$ ,  $\alpha = 2$  and  $(V_0)_{\text{Vir}} = 980 \text{ km s}^{-1}$ . Using  $V_0$  and  $\cos \Theta$  we then solve from the Peebles model the kinematical distance (Eq. (2) in BGPT86), presuming an infall velocity  $v_0 = 150 \text{ km s}^{-1}$ . In order to get a regular, uniform grid for the solutions  $d_{\text{kin}}$  we interpolate for each  $d_{\text{kin}}$  (grid) the corresponding value of  $d_t$ . The relative error  $\epsilon = 100 \times (d_t - d_{\text{kin}})/d_{\text{kin}}$  is shown as contours of equal error in the upper panels of Fig.

14. The zero-error curves are plotted as dashed lines, positive errors as solid lines and negative errors as dotted lines. Each curve reflects an increase (decrease) in the error by one percent.

The lower zero-error line represents the tangential points where the infall velocity is perpendicular to the line-of-sight thus cancelling out. On the upper zero-error line are the points which with the LG and Virgo form an isosceles triangle. Now the line-of-sight components of the infall velocity of LG and each point cancel out as they are equal but of opposite signs.

We also note how the linearized model of Peebles collapses as we approach Virgo. Following tendencies are seen from Fig. 14 (upper panels). An overestimation of  $v_0$  yields too small kinematical distances  $d_{\text{kin}}$  ( $\epsilon > 0$ ) and an underestimation too large distances ( $\epsilon < 0$ ). An inaccuracy of  $\pm 50 \text{ km s}^{-1}$  yields errors of order of a few percent. Tests also show that decrease in accuracy rapidly increases the errors.

The value of  $H_0$  is determined, however, using the corrected velocity  $V_c = ((V_0)_{\text{Vir}} + v_0) \times d_{\text{kin}}$ . As the error in  $v_0$  induces an error in  $d_{\text{kin}}$  of opposite sign, we suspect the error in  $V_c$  to be smaller than in  $d_{\text{kin}}$ . The lower panels in Fig. 14 show that this indeed is the case. Now the error-curves are based on  $\epsilon = 100 \times (V_c(\text{input}) - V_c(\text{guess}))/V_c(\text{guess})$ . In particular, in regions used for the plateau the errors are now of order of one percent or smaller. Though being rather restricted, this experiment helps one to understand why the value of  $H_0$  is so insensitive to  $v_0$ .

#### 7.1.2. The effect of the Local Group infall velocity on the plateau dispersion

The results above showed the insensitivity of  $H_0$  on the velocity model used. However, for the model to have some validity, its influence should be seen somewhere. From previous subsection we expect the dispersion of  $\log H_0$  in the plateau to be larger when incorrect velocities for Local Group infall  $v_0$  is used. In Fig. 15 the dispersion  $\sigma_{\log H}$  is plotted as a function of  $v_0$  for the adopted Virgo observed velocity  $(V_0)_{\text{Vir}} = 980 \text{ km s}^{-1}$ . The value of  $\sigma_{\log H_0}$  is derived from the real plateau data, choosing the plateau limit strictly enough so that, regardless of the value of  $v_0$ , all the data points still lie in the unbiased region.

The best value of the LG infall is then given by the minimum of the observed  $\sigma_{\log H}(v_0)$ -curve. From Fig. 15 we get  $v_0 = 225 \pm 45 \text{ km s}^{-1}$  and  $v_0 = 185 \pm 40 \text{ km s}^{-1}$  using diameter and magnitude TF relations respectively. The  $1 \sigma$ -limits have been calculated by multiplying the minimum dispersion by  $\sqrt{N/(N-1)}$ . Our standard value  $v_0 = 150 \text{ km s}^{-1}$  is within  $2 \sigma$  of these values. Agreement with the infall velocity preferred by Tammann et al. (1996) ( $V_0 = 220 \text{ km s}^{-1}$ , see Table 7) is even better.

### 7.2. Influence of the adopted galactic absorption

Changing the value of the galactic extinction  $a_g$  affects the derived Hubble constant. Smaller values lead to larger derived distances, and one obtains finally a lower value for  $H_0$ . It has been shown in Paturel et al. (1996), that the RC2 and the RC3 (Burstein-Heiles) systems for correcting galactic extinc-

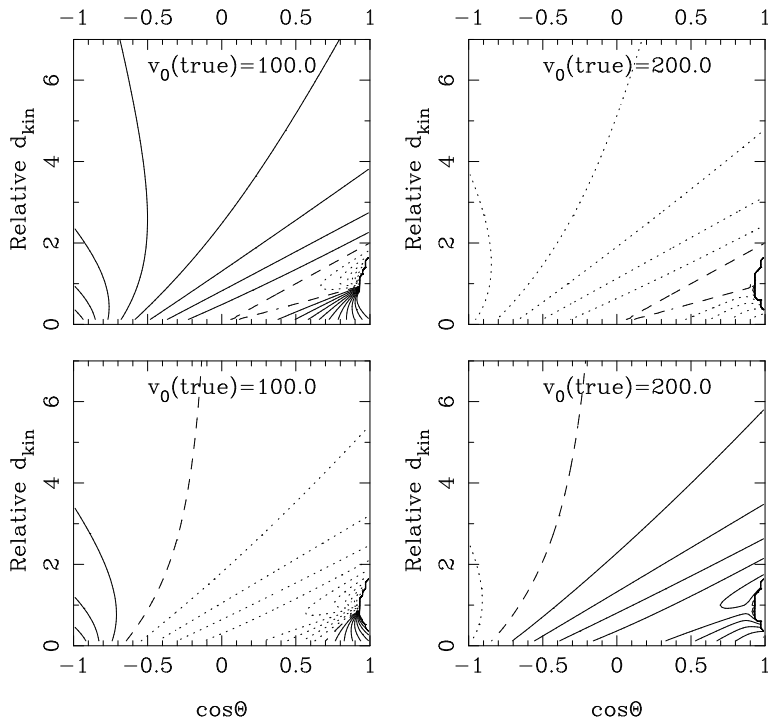


**Fig. 14.** Upper panel: the relative errors of kinematical distances obtained with the Peebles’s model, for objects with different angular distances  $\Theta$  from Virgo and different radial velocities  $V_0$ . On the left we show the error contours when the true infall velocity is  $50 \text{ km s}^{-1}$  lower, and on the right  $50 \text{ km s}^{-1}$  higher than the used value  $v_0 = 150 \text{ km s}^{-1}$ . Lower panel: now the error contours refer to the error in  $V_{\text{corr}}$ . Dashed lines represent the zero-error curves

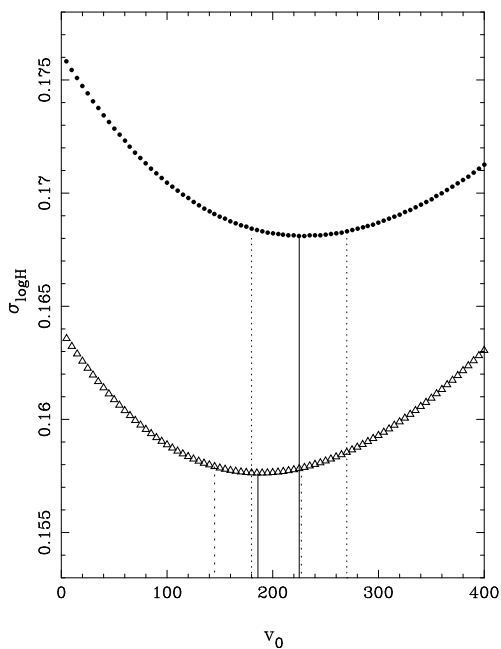


**Fig. 15.** Plateau dispersion with different values of  $v_0$ . Diameter relation has lower values of  $\sigma_{\log H_0}$  (triangles). We have also marked the minimum of the curve and the  $1 \sigma$  limits.

tion differ essentially by a simple shift of roughly  $0.18 \text{ mag}$  reflecting the assumed Galactic Pole extinction ( $a_g(\text{RC2}) \simeq 0.18 + a_g(\text{B-H})$ ). In the present paper,  $H_0$  is calculated using the RC2 system as it is available for the whole sky. Also, there is evidence from stellar reddening and interstellar polarization, that the Pole extinction may approach the RC2 value (Teeriko-

rpi, 1990, Berdyugin, Snare, and Teerikorpi, 1995, Berdyugin and Teerikorpi, 1996). Using B-H corrections, the Hubble constant is 8% (with magnitude, 4% using the diameter TF relation) smaller than when the RC2 system is used, hence,  $H_0$  becomes 49.2 with magnitudes, and 54.5 with diameters.

### 7.3. Influence of the absolute calibration

Special attention should be paid to the completeness of the calibrator sample. This sample, fixing the absolute TF zero-points and thus leading to a definite value of the Hubble constant, should, as for field galaxies, provide unbiased  $\langle M \rangle_p$  or  $\langle \log D \rangle_p$ , and be equivalent to a volume-limited sample. We studied this completeness in several ways, according to absolute diameter, absolute magnitude, and  $\log V_m$  values. Also TF residuals in both diameter and magnitude TF relations were investigated. Fig. 16 shows these parameters against the “true” Cepheid distance scale. No evidence was found for any correlation of any of these parameters with distance. We computed also a normalized distance diagram for the calibrator sample (Fig. 17), and it appears that there is no deviation from a plateau region. All of this allows us to consider the calibrator sample close to volume-limited in its statistical properties. This is not so unexpected because the galaxies have been selected for Cepheid-detection and measurement primarily on the basis of their resolution into stars.

However, group members corresponding to Table 2 seem to have a slightly different behaviour than objects of the pure Cepheid sample (Table 1). On average, their luminosity or size appears a little smaller than the mean value derived from the pure Cepheid sample, and tends to make  $H_0$  a few per cent greater. This is indeed expected from the way we generally col-

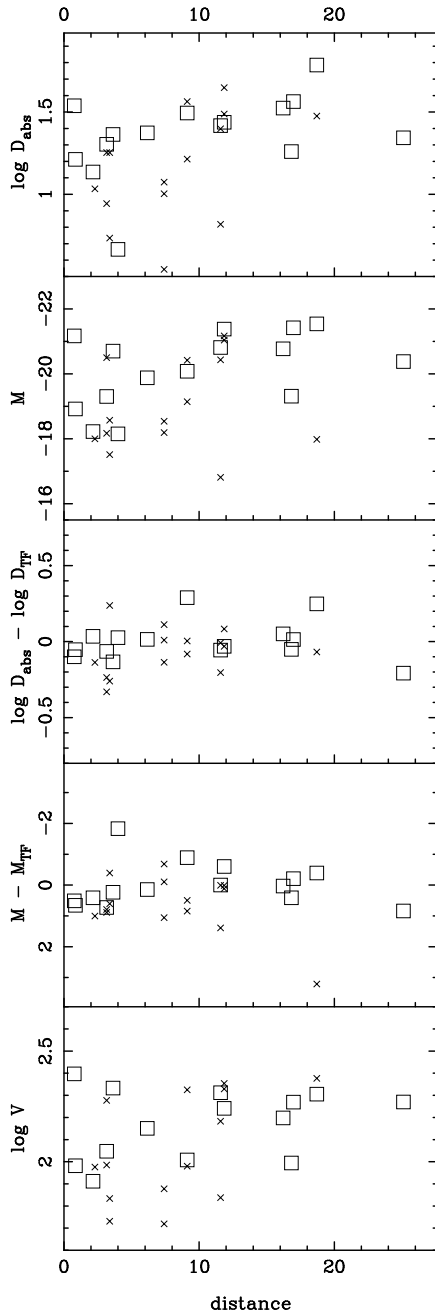


**Fig. 16.** Different parameters of the calibrator galaxies vs. their distance in Mpc. Primary (Cepheid) calibrators are plotted with squares, group calibrators with crosses. Absolute diameters and magnitudes are shown in two top panels, following them are the corresponding residuals with respect to values obtained from the TF relations. In the bottom panel the rotational velocities  $\log V_m$  are plotted.

lect group members, a method suffering from a volume effect: if one selects the objects within a certain solid angle, one collects naturally more points from the back side of the group than from its front side. The resulting average distance over all the selected group members is then greater than the true distance of the group. That is just what happens when we assign to a putative group member the Cepheid distance of another group member. Consequently, the distances for these objects being slightly

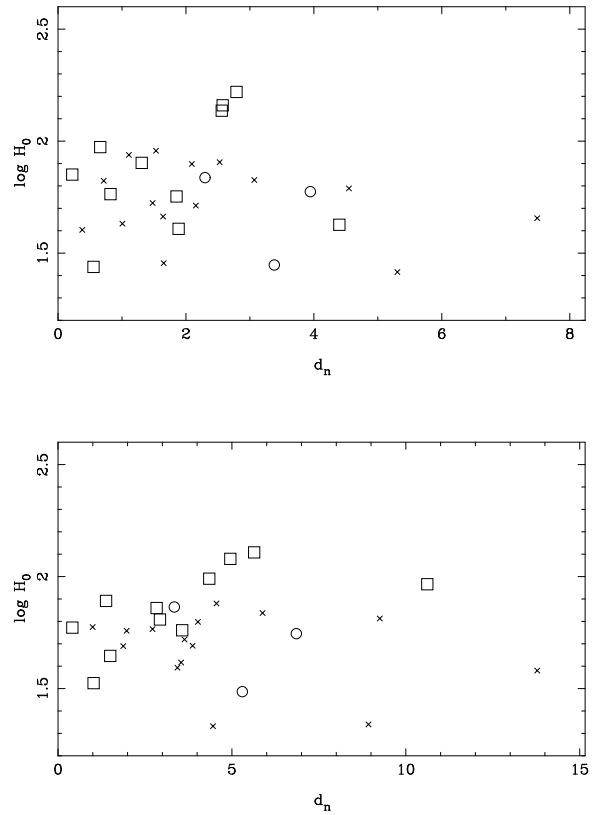


**Fig. 17.** “Plateau diagrams” (cf. Figs. 2, and 6) for calibrators. Primary and group calibrators are denoted similarly as in Fig. 16, except for Virgo galaxies, which are plotted with circles (as in Fig. 13).

under-estimated (on average), the resulting absolute calibration provides a slightly too large value of  $H_0$ . Using only the group selected calibrators we obtained  $H_0 = 66.5$  and  $H_0 = 70.9$  with diameters and magnitudes respectively. One can but hope, that in the future more HST time is allocated to field spirals. Direct Cepheid distances for these putative group members would be of great interest in order to complete the present study.

#### 7.4. Concluding remarks

One of the main purposes of the KLUN-project has been to collect a large sample of several thousand galaxies which can be analyzed by the method of normalized distances. The resulting unbiased plateau set of 400 galaxies is now ten times larger than in 1986. At the same time it is one of the largest samples of field galaxies used to derive  $H_0$ . It also reaches much greater redshifts, being well populated up to  $2000 - 3000 \text{ km s}^{-1}$ .

We report below some other novel features of the present analysis:

- for the first time, a type-dependent TF relation was used, which improves the accuracy of derived B-band TF distances
- both diameter and magnitude TF relations were used in parallel

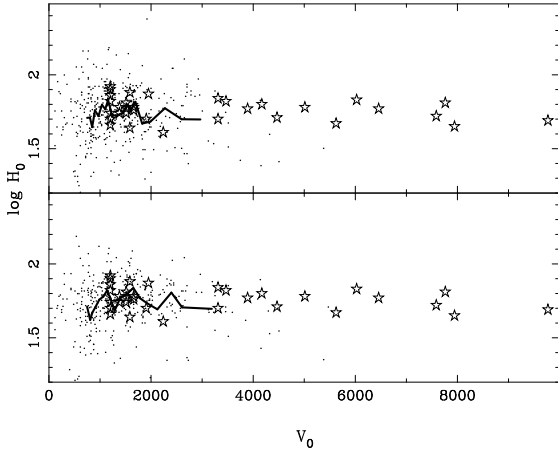


**Fig. 18.** Plateau galaxies (dots) and type Ia supernovae (stars) in a  $\log H_0$  vs.  $V_0$  diagram. The line corresponds to average value of plateau galaxies. Diameter relation used on the top, magnitudes on the bottom.

- a new method was presented for estimating the Local Group infall from the dispersion of  $\log H_0$  in the plateau
- simulations were used to show that the Hubble constant is not sensitive to the Virgo cluster velocity parameters
- the sensitivity of  $H_0$  to different infall models was checked
- we calculated analytically what portion of the total sample is the useful unbiased subsample in a normalized distance diagram
- we checked and studied the statistical properties of the primary calibrator sample, and discussed its influence on the derived Hubble constant.

It could be argued that the velocity range of the KLUN sample again provides only a local value for the Hubble constant. However, results from farther reaching standard candles also calibrated using Cepheid galaxies, the type Ia supernovae, confirm this value for larger redshifts.

In Fig. 18 we have plotted our unbiased plateau galaxies together with SNIa from Sandage et al. (1996) in an  $H_0$  vs.  $V_0$  diagram. The agreement between the two samples is good: In the lower radial velocities both have a larger dispersion, partly due to the larger relative importance of the peculiar velocities. At larger  $V_0$  the data points become fewer, but converge quite well to a mutual value of  $H_0 \approx 56$  ( $\log H_0 \approx 1.75$ ).

The value of  $H_0$  given by the SNe is of course dependent on the calibration of the method. The SNIa calibration is also based on Cepheid measurements, so we expect no systematical differences between SN and TF results from there. Our results are also in agreement with the conclusions of the "Triple-Entry-Correction" method presented for field galaxies in Sandage (1988b, 1994b), and for clusters in Sandage, Tammann, and Federspiel (1995).

Together with the recent Cepheid distances, Tully-Fisher  $B_t^0$  and  $\log D_{25}$  relations and the normalized distance method provide a firm unbiased value of the Hubble constant from field galaxies:  $H_0 = 55 \pm 5 \text{ km s}^{-1} \text{ Mpc}^{-1}$ .

*Acknowledgements.* We have made use of data from the Lyon-Meudon Extragalactic Database (LEDA) compiled by the LEDA team at the CRAL-Observatoire de Lyon (France).

We are very grateful to Allan Sandage for his detailed and useful comments.

## Appendix A: adding new calibrators

Here we provide formulae for calculating  $H_0$  when new galaxies are added in the calibrator sample.

Following the results of a study on the type dependence of TF relation (Theureau et al. 1997), we assume that the relations of different Hubble types have a common slope. Type dependence is observed in the zero-point differences of the relations ( $M$  or  $\log D = a \log V_m + b(T)$ ). Using the slope derived for the field sample we calibrate the zero-points,

$$b_c(6) = \frac{\sum(M' - a \log V_m)}{n} . \quad (\text{A.1a})$$

In the equation above,  $n$  is the number of calibrators, all of them shifted to a common type ( $T = 6$ ) by

$$M' = M + b(6) - b(T) = B_t^0 - \mu + b(6) - b(T) . \quad (\text{A.2a})$$

Equivalently, using the diameters:

$$b_c(6) = \frac{\sum(\log D_{\text{abs}}' - a \log V_m)}{n} , \quad (\text{A.1b})$$

and

$$\log D_{\text{abs}}' =$$

$$\log D_{25} + 0.2(\mu - 25) + \log \left( \frac{\pi}{180 \cdot 216000} \right) + 3 + b(6) - b(T). \quad (\text{A.2b})$$

When a new calibrator is added, we get a new value for  $b_c(6)$  simply by

$$b_{c,\text{new}}(6) = \frac{nb_{c,\text{old}}(6) + M' - a \log V_m}{n + 1} , \quad (\text{A.3})$$

or we can calculate

$$\Delta b = b_{c,\text{new}}(6) - b_{c,\text{old}}(6) = \frac{M' - a \log V_m - b_{c,\text{old}}(6)}{n + 1} . \quad (\text{A.4})$$

Hubble constant for the field sample is calculated from mean of logarithmic values (averaged over the unbiased 'plateau' sample):

$$\langle \log H_0 \rangle = \frac{\sum \log H_0}{N} = \frac{\sum [\log V_0 - 0.2(B_t^0 - a \log V_m - b_c(T) - 25)]}{N} . \quad (\text{A.5a})$$

When a new calibrator is introduced, and corresponding  $\Delta b$  has been calculated, we get

$$\langle \log H_0 \rangle_{\text{new}} = \langle \log H_0 \rangle_{\text{old}} + 0.2 \Delta b ,$$

giving

$$H_{0,\text{new}} = H_{0,\text{old}} \cdot 10^{0.2\Delta b} . \quad (\text{A.6a})$$

Correspondingly, for diameters:

$$\langle \log H_0 \rangle = \frac{\sum [\log V_c + \log D_{25} - a \log V_m - b_c(T) + \log \left( \frac{\pi}{180 \cdot 216000} \right) + 2]}{N} , \quad (\text{A.5b})$$

$$H_{0,\text{new}} = H_{0,\text{old}} \cdot 10^{-\Delta b} . \quad (\text{A.6b})$$

In conclusion: when a new Cepheid distance is announced, the reader may substitute values of  $B_1^0$  and  $\log V_m$  from table 3, and TF-parameters  $a$  and  $b(T)$  from section 5 to Eqs. (A.2) and (A.4). With  $\Delta b$  thus obtained one gets a new value for  $H_0$  (Eq. A.6).

## References

- Berdyugin, A., Snare, M.-O., Teerikorpi, P., 1995, A&A 294, 568  
 Berdyugin, A., Teerikorpi, P., 1996, A&A (in Press)  
 Bosma, A., Freeman, K., 1993, AJ 106, 1394  
 Bottinelli, L., Gouguenheim, L., Paturel, G., 1982, A&AS 47,171  
 Bottinelli, L., Gouguenheim, L., Paturel, G. Teerikorpi, P., 1986, A&A 156, 157 (BGPT86)  
 Bottinelli, L., Gouguenheim, L., Paturel, G. Teerikorpi, P., 1988, ApJ 328, 4  
 Bottinelli, L., Gouguenheim, L., Fouqué, P., Paturel, G., 1990, A&AS 82, 391  
 Bottinelli, L., Durand, N., Fouqué, P. et al., 1992, A&AS 93, 173  
 Bottinelli, L., Durand, N., Fouqué, P. et al., 1993, A&AS 102, 57  
 Bottinelli, L., Gouguenheim, L., Paturel, G., Teerikorpi, P., 1995, A&A 296, 64  
 Di Nella, H., Paturel, G., Walsh, A. et al, 1996, A&A (submitted)  
 Ekholm, T., 1996, A&A 308,7  
 Faber, S., Burstein, D., 1988, in Large Scale Motions in the Universe, eds. V. Rubin and G. Coyne, Princeton University Press, Princeton, p.115  
 Federspiel, M., Sandage, A., Tammann, G., 1994, ApJ 430, 29  
 Fouqué, P., Paturel, G., 1985, A&A 150, 192  
 Fouqué, P., Bottinelli, L., Gouguenheim, L., Paturel, G., 1990, ApJ 349,1  
 Fouqué, P., Durand, N., Bottinelli, L., Gouguenheim, L., Paturel, G., 1992, Monographies de la base de donnees extragalactiques No3, Lyon  
 Freedman, W., Madore, B., 1988, ApJ 332, L63  
 Freedman, W., Madore, B., 1990, ApJ 365, 186  
 Freedman, W., Wilson, C., Madore, B. et al., 1991, ApJ 372, 455  
 Freedman, W., Madore, B., Hawley, S. et al., 1992, ApJ 396, 80  
 Freedman, W., Madore, B., Mould, J. et al., 1994a, Nature 371, 757  
 Freedman, W., Hughes, S., Madore, B. et al., 1994b, ApJ 427, 628  
 Giovanelli, R., 1996, in The Extragalactic Distance Scale, eds. M. Livio, M. Donahue, N. Panagia, Cambridge University Press, Cambridge (in press)  
 Huchra, J., 1988, in The Extragalactic Distance Scale, eds. S. van den Bergh, C. Pritchett, ASP conf. series 4, 257  
 Kelson, D., Illingworth, G., Freedman, W. et al., 1996, ApJ 436, 26  
 Kennicutt, R., Freedman, W., Mould, J., 1995, AJ 110, 1476  
 Kraan-Korteweg, R., 1986, A&AS 66, 255  
 Lynden-Bell, D., Faber, S., Burstein, D. et al., 1988, ApJ 326, 19  
 Mould, J., Aaronson, M., Huchra, J., 1980, ApJ 238, 458  
 Paturel, G., Fouqué, P., Bottinelli, L., Gouguenheim, L., 1989, A&AS 80, 299  
 Paturel, G., Bottinelli, L., Fouqué, P., Gouguenheim, L., Teerikorpi, P., 1990, The Messenger 62, 8  
 Paturel, G., Fouqué, P., Buta, R., Garcia, A., 1991a, A&A 243, 319  
 Paturel, G., Petit, C., Kogoshvili, N. et al., 1991b, A&AS 91, 371  
 Paturel, G., Bottinelli, L., Gouguenheim, L., 1994a, A&A 286, 768  
 Paturel, G., Bottinelli, L., Di Nella, H. et al., 1994b, A&A 289, 711  
 Paturel, G., Garnier, R., Petit, C., Marthinet, M., 1996, A&A 311, 12  
 Paturel, G. et al. 1997, (in press)  
 Peebles, P., 1976, ApJ 205, 318  
 Pierce, M., Welch, D., McClure, R. et al., 1994, Nature 371, 385  
 Rawson, D. et al., 1996, ApJ (in preparation)  
 Saha, A., Sandage, A., Labhardt, L. et al., 1995, ApJ 438, 8  
 Saha, A. et al., 1996a, ApJ (in press)  
 Saha, A. et al., 1996b, ApJ (in press)  
 Sandage, A., 1988a, ApJ 331, 583  
 Sandage, A., 1988b, ApJ 331, 605  
 Sandage, A., 1994a, ApJ 430, 1  
 Sandage, A., 1994b, ApJ 430, 13  
 Sandage, A., Tammann, G., Federspiel, M., 1995, ApJ 452, 1  
 Sandage, A., Saha, A., Tammann, G. et al., 1996, ApJ (in press)  
 Silbermann, N., Harding, P., Madore, B. et al., 1996a ApJ (in press)  
 Silbermann, N., Harding, P., Madore, B. et al., 1996b ApJ (in preparation)  
 Simien, F., de Vaucouleurs, G., 1986, ApJ 302, 564  
 Tammann, G., 1987, in Observational Cosmology, IAU Symposium No. 124, eds. A. Hewitt G. Burbidge and L. Fang, D. Reidel Publishing Company, Dordrecht, p. 151  
 Tammann, G., Sandage, A., 1985, ApJ 294, 81  
 Tammann, G., Labhardt, L., Federspiel, M. et al., 1996, in Science with Hubble Space Telescope, eds. Benvenuti, P., Macchetto, F., Schreier, E. (preprint)  
 Tanvir, N., 1995, in Science with Hubble Space Telescope -meeting (private communication)  
 Tanvir, N., Shanks, T., Ferguson, H., Robinson, D., 1995, Nature 377, 27  
 Teerikorpi, P., 1975, A&A 45, 117  
 Teerikorpi, P., 1984, A&A 141, 407  
 Teerikorpi, P., 1990, A&A 235, 362  
 Teerikorpi, P., 1995, Astrophys. Lett. Comm., 31, 263  
 Theureau, G., Hanski, M., Teerikorpi, P. et al., 1997, A&A (in press)  
 Tully, B., Fouqué, P., 1985, ApJS 58, 67  
 Vaucouleurs, G., de, Vaucouleurs, A., de, Corwin, H.G. Jr, 1976, Second Reference Catalog of Bright Galaxies, University of Texas Press, Austin (RC2)  
 Vaucouleurs, G., de, Vaucouleurs, A., de, Corwin, H.G. Jr, Buta, R.J., Paturel, G. Fouqué, P., 1991, Third Reference Catalog of Bright Galaxies, Springer-Verlag (RC3)  
 Vaucouleurs, G. de, 1995, Astrophysical Letters and Communications 31, 231 (Proceedings: The World of Galaxies II)  
 Yahil, A., Tammann, G., Sandage, A., 1977, ApJ 217, 903  
 Yahil, A., Sandage, A., Tammann, G., 1980, in Physical Cosmology, eds. R. Balian, J. Adouze, and D. Schramm, North-Holland, Amsterdam, p.127  
 This article was processed by the author using Springer-Verlag L<sup>A</sup>T<sub>E</sub>X A&A style file L-AA version 3.